INSTITUTE OF PHYSICS PUBLISHING JOURNAL OF PHYSICS D: APPLIED PHYSICS

J. Phys. D: Appl. Phys. **34** (2001) 1769–1778 www.iop.org/Journals/jd PII: S0022-3727(01)19284-3

Role of long-lived $N_2(X^1\Sigma_g^+, v)$ molecules and $N_2(A^3\Sigma_u^+)$ and $N_2(a'^1\Sigma_u^-)$ states in the light emissions of an N_2 afterglow

J Loureiro[1], P A Sá[2] and V Guerra[1]

[1] Centro de Física dos Plasmas, Instituto Superior Técnico, 1049-001 Lisboa, Portugal
[2] DEEC, Faculdade de Engenharia, Universidade do Porto, 4200-465 Porto, Portugal

Received 23 November 2000, in final form 29 January 2001

Abstract

The enhancement of $N_2(B\,^3\Pi_g)$ and $N_2^+(B\,^2\Sigma_u^+)$ states, responsible by the emission bands for the 1^+ and 1^- systems of N_2, in the short-lived afterglow of a flowing N_2 microwave discharge at $\omega/(2\pi) = 433$ MHz is investigated by modelling. It is shown that pronounced maxima for both emissions are obtained downstream from the discharge by assuming the formation of $N_2(A\,^3\Sigma_u^+)$ and $N_2(a'\,^1\Sigma_u^-)$ states by collisions of $N_2(X\,^1\Sigma_g^+, v)$ molecules in highly vibrational levels with $N(^4S)$ atoms. Other channels that can also produce the emissions are investigated as well, but the common factor in all of them is the role played by the vibrationally excited $N_2(X,v)$ molecules in levels >35. During the relaxation process a pumping-up effect for the vibrational quanta at the higher vth levels occurs as a result of near-resonant V–V energy-exchange collisions, that produces a rise in the observed peaks for the N_2 electronic states in the flowing afterglow.

1. Introduction

The study of flowing N_2 microwave discharges is a pressing problem nowadays due to the large efficiency of these systems in producing N atoms for metallic nitriding by dissociation of nitrogen molecules [1–3]. The flow of neutral N atoms so obtained is used to nitride workpieces positioned downstream from the plasma where only electrically neutral species remain [4–6]. With this aim and in order to achieve a full characterization of both the early and remote afterglow regions, spectroscopic observations of the most intense bands of N_2 have been systematically carried out in recent years [2, 7–9]. In particular, it has been observed that flowing N_2 discharges produce the so-called pink afterglow, i.e. the emission bands of the first negative system of N_2 associated with the transition $N_2^+(B\,^2\Sigma_u^+ \rightarrow X^2\Sigma_g^+)$, downstream from the discharge in the short-lived afterglow region, while the characteristic yellow colour associated with the first positive system $N_2(B\,^3\Pi_g \rightarrow A^3\Sigma_u^+)$ arises in the remaining zones of the afterglow up to its far-remote region.

In a previous paper [10], we have shown that once the ground-ionic state $N_2^+(X\,^2\Sigma_g^+)$ is created in the afterglow, the upper-ionic state $N_2^+(B\,^2\Sigma_u^+)$ can be populated via the near-resonant V–E energy-exchange reaction

$$N_2(X\,^1\Sigma_g^+, v \geqslant 12) + N_2^+(X\,^2\Sigma_g^+) \rightarrow N_2(X\,^1\Sigma_g^+, v-12) + N_2^+(B\,^2\Sigma_u^+) \quad (1)$$

and that the concentration of $N_2^+(B)$ presents a maximum at $t \simeq 10^{-3}$ s (in pure N_2 and $p = 2$ Torr). This behaviour results from the fact that the vibrational distribution of $N_2(X\,^1\Sigma_g^+, v)$ molecules, in levels $v \geqslant 12$, pass through a maximum during the relaxation process, due to an efficient pumping-up effect originated by vibration–vibration (V–V) energy-exchange reactions:

$$N_2(X\,^1\Sigma_g^+, v) + N_2(X\,^1\Sigma_g^+, w) \rightarrow N_2(X\,^1\Sigma_g^+, v-1) + N_2(X\,^1\Sigma_g^+, w+1). \quad (2)$$

This effect in N_2 has been primarily pointed out by Capitelli and co-workers [11] and it is a consequence of the anharmonicity of the potential-energy curve of $N_2(X)$. Although in the early-afterglow $N_2^+(B)$ ions may also be created by electron impact on $N_2^+(X)$, the contribution of this latter mechanism is always vanishingly small compared with reaction (1), even in discharge conditions [12].

On the other hand, it is well known that the ground-ionic state $N_2^+(X\,^2\Sigma_g^+)$ can be created in the afterglow, together with N_4^+ ions, by collisions between the metastable states $N_2(A\,^3\Sigma_u^+)$

and $N_2(a'\,^1\Sigma_u^+)$ according to the following Penning ionization reactions [13–16]:

$$N_2(A\,^3\Sigma_u^+) + N_2(a'\,^1\Sigma_u^-) \rightarrow N_2(X\,^1\Sigma_g^+) + N_2^+(X\,^2\Sigma_g^+) + e \quad (3)$$

$$N_2(a'\,^1\Sigma_u^-) + N_2(a'\,^1\Sigma_u^-) \rightarrow N_2(X\,^1\Sigma_g^+) + N_2^+(X\,^2\Sigma_g^+) + e. \quad (4)$$

These mechanisms are dominant even in a low-pressure stationary N_2 discharge, in which ionization by electron impact also occurs [17], either under the form of direct electron ionization on $N_2(X)$ or by electron stepwise ionization on $N_2(A)$ and $N_2(a')$.

However, neither $N_2(A\,^3\Sigma_u^+)$ nor the $N_2(a\,^1\Sigma_u^-)$ states can be produced in the discharge and carried out to the post-discharge, since the emission bands of 1^- and 1^+ systems increase in the afterglow after a dark zone positioned at the end of the discharge. This fact seems to indicate unambiguously that both metastables need to be created in the afterglow, producing the ionic species responsible for the emission bands of the 1^- system, as well as the $N_2(B\,^3\Pi_g)$ and $N_2(C\,^3\Pi_u)$ states responsible for the emissions of 1^+ and 2^+ systems of N_2, respectively.

Here, in order to analyse the conditions for the enhancement of $N_2^+(B\,^2\Sigma_u^+)$ and $N_2(B\,^3\Pi_g)$ concentrations in the post-discharge, the effects of several mechanisms leading to the formation of N_2 electronic states have been investigated by modelling the nitrogen afterglow of a microwave discharge at $\omega/(2\pi) = 433$ MHz, for $p = 2.56$ Torr (i.e. 340 Pa) and $p = 10$ Torr. Our study shows that an increase of both $[N_2^+(B)]$ and $[N_2(B)]$ is observed when we assume that the N_2 electronic states, $A\,^3\Sigma_u^+$, $B\,^3\Pi_g$ and $a'\,^1\Sigma_u^-$, are created in the post-discharge, as a result of collisions between vibrationally excited molecules $N_2(X\,^1\Sigma_g^+, v)$, at higher vth levels, and long-lived $N(^4S)$ atoms. The increase in the peaks associated with both emissions (1^- and 1^+ systems) takes place due to the fact that during the relaxation process the near-resonant V–V energy-exchanges induce the quanta at the higher vth levels (the so-called V–V pumping-up effect) to climbing the vibrational ladder. These near-resonant V–V exchanges are far more effective in transfer vibrational quanta than the non-resonant V–V and vibration–translation (V–T) energy-exchange collisions. However, the concentration of $N(^4S)$ atoms remains practically unchanged from the discharge to the post-discharge region, as a result of the large characteristic times for $N(^4S)$ losses on the wall and gas-phase (three-body) recombination. Nevertheless, an enhancement of $[N(^4S)]$ along the post-discharge may occur, due to a decrease in the gas temperature.

2. Kinetic model

The theoretical formulation used in this paper for a microwave discharge and its afterglow is close to that employed in [10], with some exceptions that will be discussed in the text. With respect to the model for the discharge, we solve the stationary homogeneous electron Boltzmann equation for the microwave field, using the effective-field approximation [18], coupled to a system of stationary rate-balance equations for the vibrational levels $N_2(X\,^1\Sigma_g^+, v)$, different N_2 electronic states ($A\,^3\Sigma_u^+$, $B\,^3\Pi_g$, $B'\,^3\Sigma_u^-$, $C\,^3\Pi_u$, $a'\,^1\Sigma_u^-$, $a\,^1\Pi_g$, and $w\,^1\Delta_u$), $N(^4S)$ atoms and $N_2^+(X\,^2\Sigma_g^+)$, $N_2^+(B\,^2\Sigma_u^+)$ and N_4^+ ions. The maintenance electric field is self-consistently determined by equalling, under steady-state conditions, the total rate of ionization with the rate of electron loss by ambipolar diffusion to the wall plus electron–ion recombination. The ionization processes included are direct and stepwise electron impact ionization, the latter under the form of collisions of electrons on the $N_2(A)$ and $N_2(a')$ states, and reactions (3) and (4) for collisions between metastable states. The reader should refer to [10, 17] for details about our reference model as well as for the collisional data used in this paper. The present set of equations allows us to determine the electron energy distribution function (EEDF), the various energy-averaged quantities obtained from the EEDF, such as the electron rate coefficients for excitation, the vibrational distribution function (VDF) of $N_2(X,v)$ molecules, and the concentrations of various N_2 electronic states, $N(^4S)$ atoms, and different ionic species.

The evolution of the concentrations in the post-discharge is analysed by considering the relaxation of the previous set of coupled kinetic master equations for the discharge, plus some specific reactions for the production of $N_2(A\,^3\Sigma_u^+$, $B\,^3\Pi_g$, $a'\,^1\Sigma_u^-)$ states in the post-discharge, considered here to investigate the optimum conditions for the enhancement of the peaks of 1^- and 1^+ systems of N_2 as observed in [2, 7, 8]. The present simulation is carried out neglecting processes resulting from electron impact in the afterglow. Although not absolutely vanishing, electron collisions cannot be responsible for the appearance of the observed maxima in the afterglow [19], so that their neglect is absolutely justified within the purposes of the present study.

Several mechanisms have been investigated here to check their possibilities in creating the maxima for 1^- and 1^+ emissions observed in the afterglow.

(i) Creation of $N_2(A\,^3\Sigma_u^+)$ metastable states in the post-discharge through collisions between two vibrationally excited $N_2(X,v)$ molecules, in levels $v \geqslant 12$, promoting the transfer from vibrational to electronic excitation:

$$N_2(X\,^1\Sigma_g^+, v \geqslant 12) + N_2(X\,^1\Sigma_g^+, v \geqslant 12) \rightarrow N_2(A\,^3\Sigma_u^+) + N_2(X\,^1\Sigma_g^+, v = 0). \quad (5)$$

This reaction is forbidden by spin conservation rules and its cross section should be small. This is in line with measurements realised in [20] for the rate coefficients for quenching the $v' = 0$ and $v' = 1$ levels of $N_2(A)$ by $N_2(X,v = 0)$, in which the values $< 2.6 \times 10^{-18}$ cm^3 s^{-1} and 3.8×10^{-17} cm^3 s^{-1} for $v' = 0$ and $v' = 1$, respectively, have been determined. The application of detailed balance to these values gives a rate coefficient of the order of 10^{-18}–10^{-17} cm^3 s^{-1} for reaction (5). Here, we have analysed the effect of reaction (5) in the model for the post-discharge using values of this order, as well as by increasing the rate coefficient up to the largest value of 10^{-16} cm^3 s^{-1} reported in [12], obtained from the data compilation [21].

(ii) Creation of $N_2(B\,^3\Pi_g)$ states in the post-discharge by collisions between two $N_2(X,v)$ molecules, in levels $v \geqslant 14$:

$$N_2(X\,^1\Sigma_g^+, v \geqslant 14) + N_2(X\,^1\Sigma_g^+, v \geqslant 14) \rightarrow N_2(B\,^3\Pi_g) + N_2(X\,^1\Sigma_g^+, v = 0). \quad (6)$$

This reaction is also forbidden by spin conservation rules, which is in agreement with the fact that the quenching of $B\,^3\Pi_g$ leads to the formation of $W\,^3\Delta_u$ and $A\,^3\Sigma_u^+$ states only [22]. Here, in the absence of more reliable information, we have used for reaction (6) the rate coefficient reported in [12], 10^{-15} cm^3 s^{-1}, once again obtained from [21].

(iii) Creation of the singlet state $N_2(a'\,^1\Sigma_u^-)$ in the post-discharge by collisions between two $N_2(X,v)$ molecules, in levels $v \geqslant 16$,

$$N_2(X\,^1\Sigma_g^+, v \geqslant 16) + N_2(X\,^1\Sigma_g^+, v \geqslant 16) \rightarrow N_2(a'\,^1\Sigma_u^-) + N_2(X\,^1\Sigma_g^+, v = 0). \quad (7)$$

This mechanism has been primarily proposed in [15], assuming the rate coefficient 2.5×10^{-15} cm^3 s^{-1}, to reconcile model predictions with measurements of N_2 ionization rates. Rate coefficients of the same order have also been assumed in [12, 23].

(iv) Production of $N_2(A\,^3\Sigma_u^+)$ metastables in the post-discharge through collisions between $N_2(X,v)$ molecules, in levels $v \geqslant 25$, and $N(^4S)$ atoms:

$$N_2(X\,^1\Sigma_g^+, v \geqslant 25) + N(^4S) \rightarrow N_2(A\,^3\Sigma_u^+) + N(^4S). \quad (8)$$

In spite of this reaction being forbidden, once again by spin conservation rules, the rate coefficient for quenching of $N_2(A)$ by N atoms, that is for the reverse reaction (8), has been measured in [24] with the value 5×10^{-11} cm^3 s^{-1}. The application of detailed balance to reaction (8) gives for the forward reaction, at resonant conditions, $k_f = 3 \times k_r = 1.5 \times 10^{-10}$ cm^3 s^{-1} [11]. However, more detailed studies on the reaction for quenching of $N_2(A)$ by N atoms have shown that $N(^2P)$ is the final product from this quenching and a rate coefficient equal to 4×10^{-11} cm^3 s^{-1} [25] for the following reaction was determined:

$$N_2(A\,^3\Sigma_u^+) + N(^4S) \rightarrow N_2(X\,^1\Sigma_g^+, 6 \leqslant v \leqslant 9) + N(^2P). \quad (9)$$

Here, in the absence in the model of the kinetics of $N(^2D)$ and $N(^2P)$ metastable and due to the fact that the measured ratio $[N(^2P)]/[N(^4S)]$ is of the order $\sim 10^{-3}$ [26], while an estimate for $[N_2(X,v \geqslant 25)]/[N_2(X,6 \leqslant v \leqslant 9)]$ gives $\sim 10^{-1}$ [10], we will assume a upper limit for the rate coefficient of reaction (8) equal to 1.5×10^{-12} cm^3 s^{-1}.

(v) Creation of $N_2(B\,^3\Pi_g)$ states in the post-discharge through collisions of $N_2(X,v)$ molecules, in levels $v \geqslant 31$, with $N(^4S)$ atoms:

$$N_2(X\,^1\Sigma_g^+, v \geqslant 31) + N(^4S) \rightarrow N_2(B\,^3\Pi_g) + N(^4S). \quad (10)$$

Owing to the same reasons as in the previous reaction leading to the formation of $N_2(A)$, the cross section of reaction (10) should be small. Here, due to a lack of data we will assume the value 10^{-12} cm^3 s^{-1} for the upper limit of the rate coefficient of reaction (10). It is worth noting that reaction (10) may be considered as a somewhat equivalent reverse reaction of

$$N_2(B\,^3\Pi_g) + N(^4S) \rightarrow N_2(X\,^1\Sigma_g^+, v \sim 20) + N(^2D) \quad (11)$$

so that in the absence of more reliable information, the magnitude assumed in this paper for the rate coefficient of reaction (10) seems to be appropriate.

(vi) Finally, we will also consider the creation of the singlet state $N_2(a'\,^1\Sigma_u^-)$ in the post-discharge by collisions of $N_2(X,v)$ molecules, in levels $v \geqslant 38$, with $N(^4S)$ atoms:

$$N_2(X\,^1\Sigma_g^+, v \geqslant 38) + N(^4S) \rightarrow N_2(a'\,^1\Sigma_u^-) + N(^4S). \quad (12)$$

This reaction is now allowed by spin conservation although it does not obey dipole selection rules. Nevertheless, there is some evidence that these rules do not apply to collisions [27]. Here, due to a lack of data we will assume the same rate coefficient, 10^{-12} cm^3 s^{-1}, as in reaction (10). We note that the existence of a similar reaction to the reverse reaction (12), although involving collisions with $N_2(X,v = 0)$ molecules instead of $N(^4S)$ atoms, has been suggested in [27], in order to account for a measured strong quenching of $N_2(a')$ state by N_2:

$$N_2(a'\,^1\Sigma_u^-) + N_2(X\,^1\Sigma_g^+, v = 0) \rightarrow N_2(X\,^1\Sigma_g^+, v = 38) + N_2(X\,^1\Sigma_g^+, v = 0). \quad (13)$$

The processes listed here for the formation of N_2 electronic states in the afterglow are inserted into a complex kinetic model with a large number of other reactions [10]. With respect to the $N_2(A\,^3\Sigma_u^+)$ and $N_2(B\,^3\Pi_g)$ states, for example, they are strongly coupled to each other through the following reactions for the quenching of one species with formation of the other:

$$N_2(A\,^3\Sigma_u^+) + N_2(X\,^1\Sigma_g^+, 5 \leqslant v \leqslant 14) \rightarrow N_2(B\,^3\Pi_g) + N_2(X\,^1\Sigma_g^+, v = 0) \quad (14)$$

$$N_2(B\,^3\Pi_g) + N_2(X\,^1\Sigma_g^+) \rightarrow N_2(A\,^3\Sigma_u^+) + N_2(X\,^1\Sigma_g^+). \quad (15)$$

These processes have the rate coefficients 2×10^{-11} cm^3 s^{-1} and $< 3 \times 10^{-11}$ cm^3 s^{-1} for reactions (14) and (15), respectively. The associated rates are by far dominant in comparison with the rates for any other process involving either $N_2(A)$ or $N_2(B)$, including the reactions discussed in this section for the formation of both states in the afterglow. Therefore, the combined effects of reactions (14) and (15) do not, in fact, constitute a populating/depopulating mechanism for $N_2(A)$ and $N_2(B)$, as they just redistribute a constant population among the triplet manifold [17].

3. Results

The results of this paper have been obtained for the post-discharge of an N_2 microwave discharge at $\omega/(2\pi) = 433$ MHz, in an $R = 1.9$ cm inner tube radius, at $p = 2.56$ Torr and 10 Torr, assuming a homogeneous electron density $n_e = 10^{11}$ cm^{-3} and gas temperature $T_g = 1000$ K, which correspond to typical experimental conditions in discharges of this type [2, 7–9]. In particular, the electron density may be varied by changing the microwave power injected into the discharge [10]. The probability for wall reassociation of $N(^4S)$ atoms in the discharge has been chosen to be $\gamma = 5 \times 10^{-4}$ [28]. Under present conditions, we obtain for the maintenance of a reduced electric field $E/N = 7.3 \times 10^{-16}$ V cm^2 and 5.2×10^{-16} V cm^2, for 2.56 Torr and 10 Torr, respectively, with N denoting the gas density, and $T_v = 11\,300$ K and 7600 K for the vibrational temperature of the lowest vth levels of the VDF, for the same two values of pressure. The kinetic model determines, among

other parameters, the fractional concentrations of all species produced in the medium. For the relative atomic concentration, for example, we determine $[N(^4S)]/[N_2] = 2.0 \times 10^{-3}$ and 4.2×10^{-4} at $p = 2.56$ Torr and 10 Torr, respectively.

The evolution of the concentrations of the various species produced in the discharge is analysed in the post-discharge, by considering the relaxation of a set of coupled time-varying kinetic master equations, assuming the neglect of processes by electron impact and a constant gas temperature $T_g = 400$ K (for which a probability $\gamma = 3.2 \times 10^{-6}$ for wall reassociation of $N(^4S)$ atoms in the post-discharge has been assumed [29]). Recent studies show that while neglecting electron collisions in the afterglow does not significantly affect the results of this paper [19], the constancy of the gas temperature along the post-discharge and, in particular, the assumption of $T_g = 400$ K at earlier moments of the afterglow [30], should be considered as a suitable approximation made here with the purpose to separate the effects of the reactions that we want to study from the temperature effects. The variation of temperature in the post-discharge will be contemplated in a future publication.

Figures 1 and 2 show the evolution of the relative concentrations $[N_2(A\,^3\Sigma_u^+)]/[N_2]$ and $[N_2(a'\,^1\Sigma_u^-)]/[N_2]$ obtained from our model, in the case of the afterglow of a microwave discharge with $p = 2.56$ Torr, when the reactions (8) and (12), respectively, are inserted. As we have seen in section 2, these reactions lead to the production of $N_2(A)$ and $N_2(a')$ states through collisions of $N_2(X\,^1\Sigma_g^+, v)$ molecules, in intermediate ($\geqslant$25) and high ($\geqslant$38) vth levels, respectively, with $N(^4S)$ atoms. In figure 1 we have considered the upper limit for the rate coefficient of reaction (8), 1.5×10^{-12} cm^3 s^{-1} (curve A), and two smaller values 1.5×10^{-14} cm^3 s^{-1} (B) and 1.5×10^{-15} cm^3 s^{-1} (C), while in figure 2 the various curves have been obtained for decreasing values of the rate coefficient of reaction (12) from our reference value, 10^{-12} cm^3 s^{-1} (curve A), down to 10^{-15} cm^3 s^{-1} (curve D). A comparison between figures 1 and 2 show that more pronounced maxima are obtained in the production of $N_2(a')$ through reaction (12), since in this latter case the vth levels participating in the process belong to the tail of the VDF, which is, in fact, the region of the VDF preferentially pumped by the non-resonant V–V energy exchanges.

In order to illustrate this mechanism of distribution of vibrational quanta, figure 3 shows the VDF calculated in the same conditions as in curve A of figure 2, for the following times in the afterglow: (A) $t = 0$; (B) 10^{-4} s; (C) 10^{-3} s; (D) 10^{-2} s; (E) 10^{-1} s. The tail of the VDF passes through a maximum at $t \sim 10^{-3}$–10^{-2} s due to the effect of near-resonant V–V energy exchanges. Owing to the anharmonicity of the potential-energy curve of $N_2(X)$, the energy difference between neighbouring vibrational levels is not the same everywhere. It decreases from the bottom to the top of the vibrational ladder. As a consequence of this, the V–V energy exchanges associated with reaction (2) are not exactly resonant and they present larger rate coefficients for the exchanges that lead to a gain of vibrational quanta for the highest levels and loss of quanta for the lowest ones. The reaction $(v, w) \rightarrow (v - 1, w + 1)$, with $w > v$, transfers energy from the vibrational to the translational mode, so that it presents a larger rate coefficient than the reverse process. The application of detailed balancing to reaction (2) allows us to

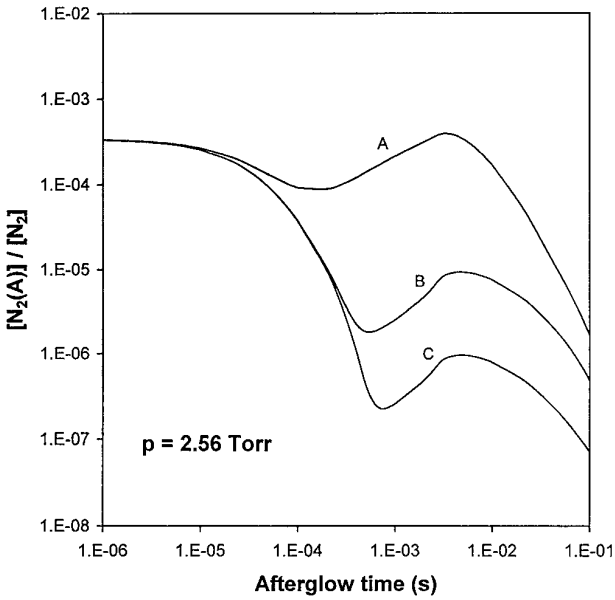

Figure 1. Temporal evolution of the fractional concentration of $N_2(A)$ metastable in the afterglow of a microwave discharge at $\omega/(2\pi) = 433$ MHz and $p = 2.56$ Torr, assuming the formation of $N_2(A)$ through the mechanism
$N_2(X, v \geqslant 25) + N(^4S) \rightarrow N_2(A) + N(^4S)$, with the rate coefficient:
(A) 1.5×10^{-12} cm^3 s^{-1}; (B) 1.5×10^{-14} cm^3 s^{-1};
(C) 1.5×10^{-15} cm^3 s^{-1}.

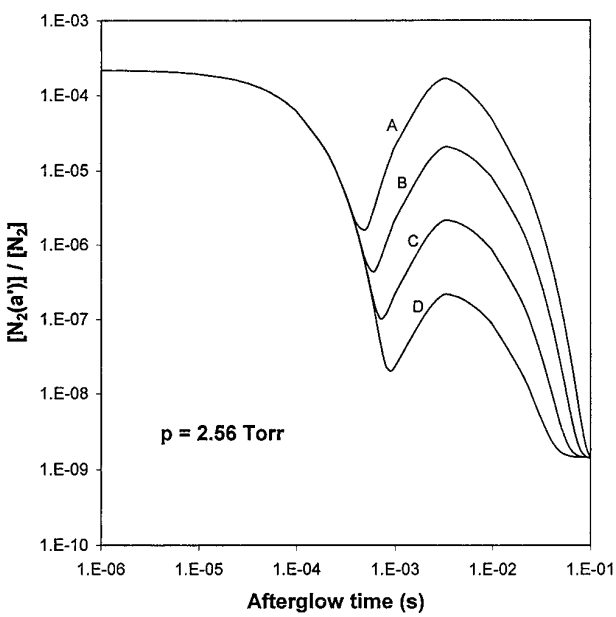

Figure 2. Temporal evolution of the fractional concentration of $N_2(a')$ state in the afterglow of a microwave discharge at $\omega/(2\pi) = 433$ MHz and $p = 2.56$ Torr, assuming the formation of $N_2(a')$ through the mechanism
$N_2(X, v \geqslant 38) + N(^4S) \rightarrow N_2(a') + N(^4S)$, with the rate coefficient:
(A) 10^{-12} cm^3 s^{-1}; (B) 10^{-13} cm^3 s^{-1}; (C) 10^{-14} cm^3 s^{-1};
(D) 10^{-15} cm^3 s^{-1}.

write the following relation between the rate coefficients for direct and reverse V–V energy-exchange processes:

$$\frac{P_{v,v-1}^{w,w+1}}{P_{v-1,v}^{w+1,w}} = \exp\left(\frac{\Delta E_{v,v-1}^{w,w+1}}{kT_g}\right) \tag{16}$$

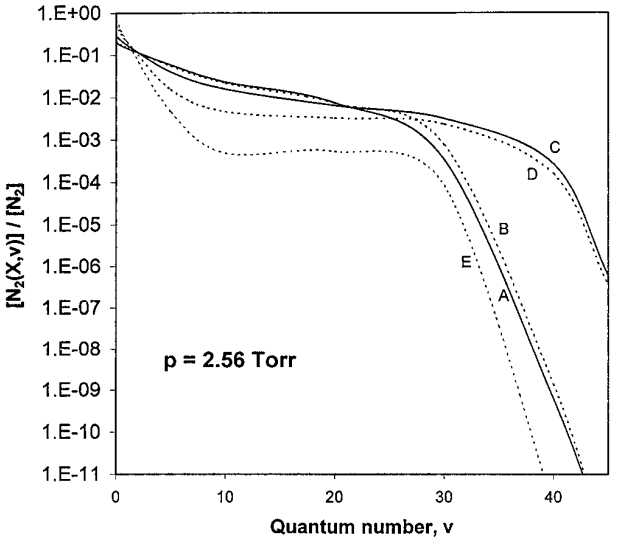

Figure 3. VDF of $N_2(X,v)$ molecules in the afterglow of a microwave discharge at $\omega/(2\pi) = 433$ MHz and $p = 2.56$ Torr, assuming the rate coefficient 10^{-12} cm^3 s^{-1} for the mechanism $N_2(X,\, v \geqslant 38) + N(^4S) \rightarrow N_2(a') + N(^4S)$, at the following times: (A) $t = 0$; (B) 10^{-4} s; (C) 10^{-3} s; (D) 10^{-2} s; (E) 10^{-1} s.

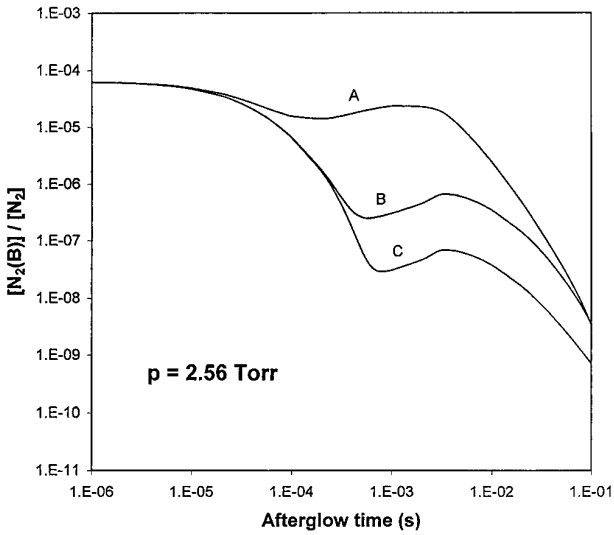

Figure 4. Temporal evolution of the fractional concentration of $N_2(B)$ in the afterglow of a microwave discharge at $\omega/(2\pi) = 433$ MHz and $p = 2.56$ Torr, assuming the formation of $N_2(A)$ through the mechanism $N_2(X,\, v \geqslant 25) + N(^4S) \rightarrow N_2(A) + N(^4S)$, with the rate coefficient: (A) 1.5×10^{-12} cm^3 s^{-1}; (B) 1.5×10^{-14} cm^3 s^{-1}; (C) 1.5×10^{-15} cm^3 s^{-1}.

where $\Delta E^{w,w+1}_{v,v-1} = (E_{v,v-1} - E_{w+1,w}) > 0$ denotes the energy transferred to the translational mode and k is the Boltzmann constant.

Whereas the relative concentration of $N_2(X,v)$ molecules in levels $v \geqslant 38$ pass through a pronounced maximum during the relaxation process at $t \sim 10^{-3}$–10^{-2} s, figure 3 shows that this effect is considerably smaller at the levels $v \sim 25$, which explains the appearance of only a smooth peak in figure 1, for the production of $N_2(A)$ states through reaction (8). Once both $N_2(A)$ and $N_2(a')$ states have been created in the afterglow, the upper states associated with the emissions of 1^+ and 1^- systems of N_2 are produced by the joint action of the interplay kinetics [10]. Figures 4–6 show the evolution of the relative concentration of $N_2(B\,^3\Pi_g)$ state, responsible for the emission of system 1^+, when the model assumes the creation of $N_2(A)$, $N_2(B)$, and $N_2(a')$ states in the afterglow through reactions (8), (10), and (12). These three mechanisms involve collisions of $N_2(X,v)$ molecules in levels higher than 25, 31 and 38, respectively, with $N(^4S)$ atoms, so that the strongest maximum is obtained for the case of reaction (12), since it preferentially depends on the tail of the VDF. In figure 4, $N_2(B)$ is created from $N_2(A)$ by reaction (14), while in figure 6 $N_2(B)$ is created from $N_2(a')$ through the reaction

$$N_2(a'\,^1\Sigma_u^-) + N_2 \rightarrow N_2(B\,^3\Pi_g) + N_2 \qquad (17)$$

with the rate coefficient 1.9×10^{-13} cm^3 s^{-1} [31, 32].

The same conclusion is valid for the 1^- system of N_2. Figure 7 shows the evolution of the fractional concentration of the upper-ionic state $N_2^+(B^2\Sigma_u^+)$ calculated from our model when it is assumed a singlet state $N_2(a'\,^1\Sigma_u^-)$ is created in the afterglow through reaction (12). Once the $N_2(a')$ state is created, it can produce the ground-ionic state $N_2^+(X\,^2\Sigma_g^+)$ through the ionizing reaction (4) followed by the production of $N_2^+(B)$ via the near-resonant V–E energy-exchange reaction (1). Since this latter mechanism involves low vth levels as low as $v \geqslant 12$, an appreciable pumping-up effect associated with

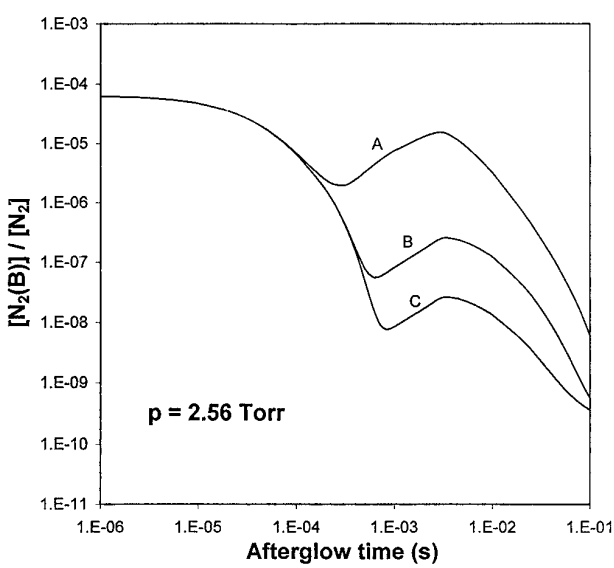

Figure 5. Temporal evolution of the fractional concentration of $N_2(B)$ in the afterglow of a microwave discharge at $\omega/(2\pi) = 433$ MHz and $p = 2.56$ Torr, assuming the formation of this state through the mechanism $N_2(X,\, v \geqslant 31) + N(^4S) \rightarrow N_2(B) + N(^4S)$, with the rate coefficient: (A) 10^{-12} cm^3 s^{-1}; (B) 10^{-14} cm^3 s^{-1}; (C) 10^{-15} cm^3 s^{-1}.

reaction (1) does not exist so that the peaks calculated for $N_2^+(X)$ and $N_2^+(B)$ are very similar. Figure 8 shows the fractional concentration of the ground-ionic state $N_2^+(X)$ calculated in the same conditions as in figures 2, 6 and 7.

Our investigations clearly show that only reactions involving highly vibrational levels, of say >35, can produce the appearance of the emissions of the 1^+ and 1^- systems of N_2 in a flowing post-discharge, in a zone localized downstream from the discharge after a dark space, as was experimentally observed in [7–9]. Figure 9 shows an example of such a

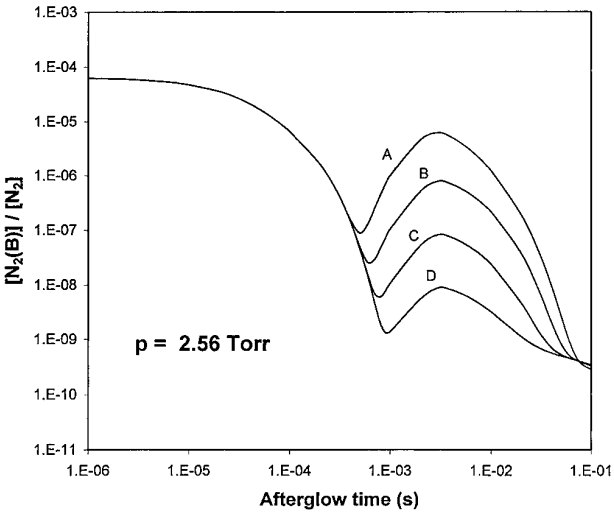

Figure 6. Temporal evolution of the fractional concentration of $N_2(B)$ in the afterglow of a microwave discharge at $\omega/(2\pi) = 433$ MHz and $p = 2.56$ Torr, assuming the formation of $N_2(a')$ through the mechanism $N_2(X, v \geqslant 38) + N(^4S) \rightarrow N_2(a') + N(^4S)$, with the rate coefficient: (A) 10^{-12} cm^3 s^{-1}; (B) 10^{-13} cm^3 s^{-1}; (C) 10^{-14} cm^3 s^{-1}; (D) 10^{-15} cm^3 s^{-1}.

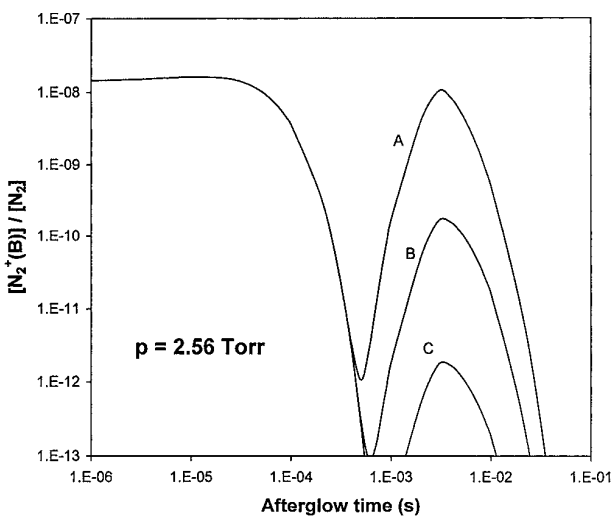

Figure 7. Temporal evolution of the fractional concentration of the upper-ionic state $N_2^+(B)$ in the afterglow of a microwave discharge at $\omega/(2\pi) = 433$ MHz and $p = 2.56$ Torr, assuming the formation of $N_2(a')$ through the mechanism $N_2(X, v \geqslant 38) + N(^4S) \rightarrow N_2(a') + N(^4S)$, with the rate coefficient: (A) 10^{-12} cm^3 s^{-1}; (B) 10^{-13} cm^3 s^{-1}; (C) 10^{-14} cm^3 s^{-1}.

situation for the 1^- system of N_2^+, measured in the short-lived afterglow of a flowing N_2 microwave discharge at $p =$ 340 Pa, with a flow rate of 1.40 slpm (standard litre per minute), generated by two similar coaxial cavities at $\omega/(2\pi) =$ 433 MHz and 2.45 GHz [8]. The intensity profiles of the 1^- system show pronounced maxima for both frequencies. A comparison of the present theoretical predictions with the intensity profiles is not possible here because the electron density in the discharge was not determined in the experiment [8], which means that the concentrations of the various species at the beginning of the afterglow are certainly not the same. However, figure 7 shows that at least a

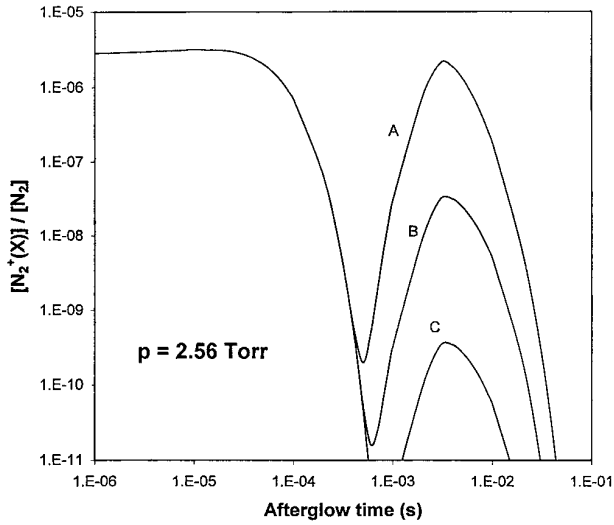

Figure 8. Temporal evolution of the fractional concentration of the ground-ionic state $N_2^+(X)$ in the same conditions and notation as in figure 7.

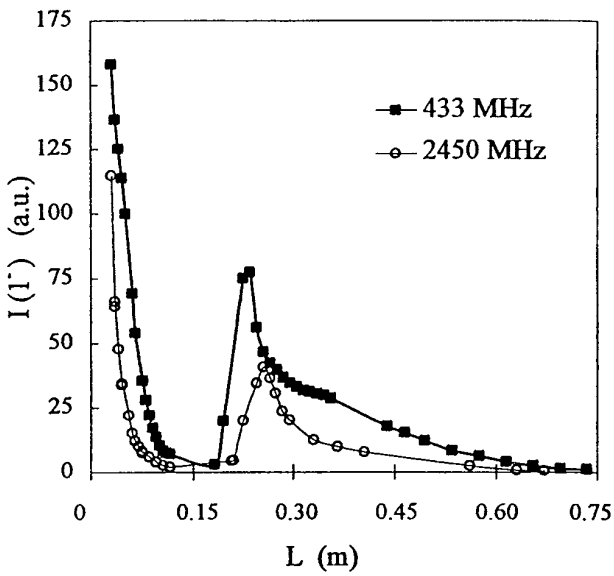

Figure 9. Intensity profiles of the 1^- system emission of N_2^+ for the frequencies 433 MHz and 2450 MHz (after Blois *et al* [8] with permission).

good qualitative agreement exists between the fractional concentration $[N_2^+(B)]/[N_2]$ calculated here and the intensity profiles of the 1^- system shown in figure 9.

On the other hand, if the production of $N_2(A)$ and $N_2(B)$ states was assumed to be by reactions (8) and (10) only slight maxima would be obtained. It follows from the present discussion that the emissions cannot also be produced by collisions between two vibrationally excited $N_2(X,v)$ molecules at intermediate levels, as in the case of reactions (5)–(7), involving collisions between two molecules in levels $v = 12$–16. In this latter case, a continuous increase in $N_2(B)$ and $N_2^+(B)$ concentrations is observed and no dark zone at the end of the discharge arises from the model.

Figures 10 and 11 show the evolution of the relative concentrations $[N_2(B)]/[N_2]$ and $[N_2^+(B)]/[N_2]$ in the

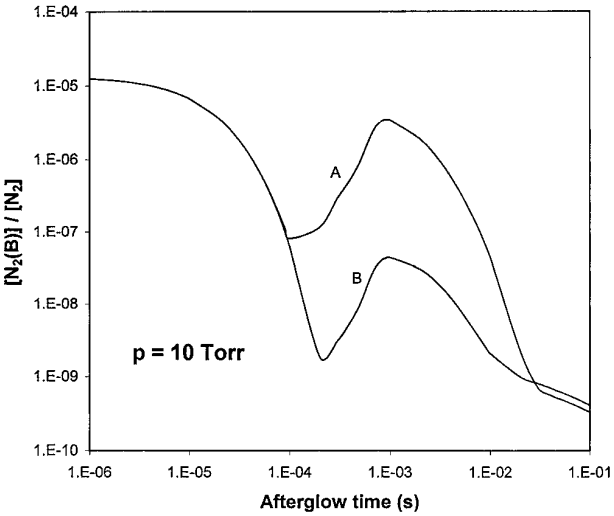

Figure 10. Temporal evolution of the fractional concentration of $N_2(B)$ state in the afterglow of a microwave discharge at $\omega/(2\pi) = 433$ MHz and $p = 10$ Torr, assuming the formation of $N_2(a')$ through the mechanism $N_2(X, v \geqslant 38) + N(^4S) \rightarrow N_2(a') + N(^4S)$, with the rate coefficient: (A) 10^{-12} cm^3 s^{-1}; (B) 10^{-14} cm^3 s^{-1}.

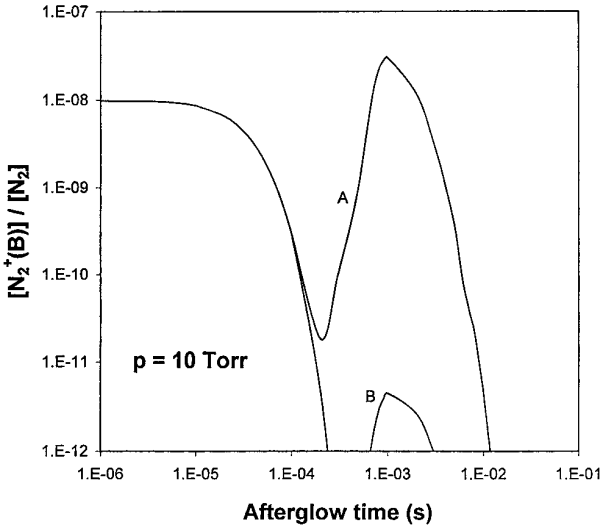

Figure 11. Temporal evolution of the fractional concentration of $N_2^+(B)$ ions in the same conditions and notation as in figure 10.

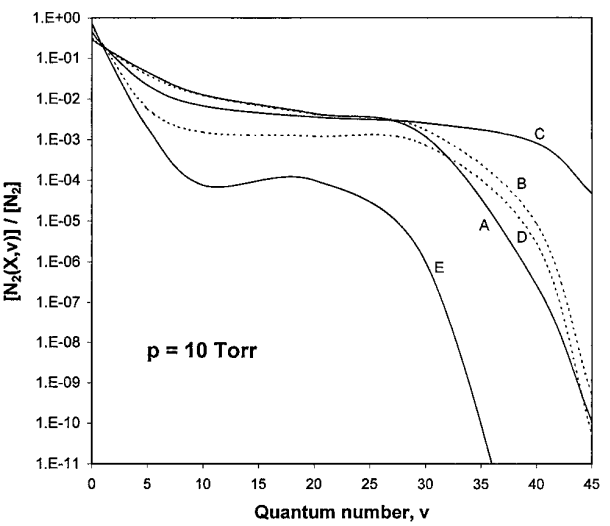

Figure 12. VDF of $N_2(X,v)$ molecules in the afterglow of a microwave discharge at $\omega/(2\pi) = 433$ MHz and $p = 10$ Torr, assuming the rate coefficient 10^{-12} cm^3 s^{-1} for the mechanism $N_2(X, v \geqslant 38) + N(^4S) \rightarrow N_2(a') + N(^4S)$, at the following times: (A) $t = 0$; (B) 10^{-4} s; (C) 10^{-3} s; (D) 10^{-2} s; (E) 10^{-1} s.

post-discharge of a flowing discharge at the higher pressure $p = 10$ Torr, assuming the creation of the singlet $N_2(a')$ state in the afterglow via reaction (12), with a rate coefficient equal to 10^{-12} cm^3 s^{-1} (curves A) and 10^{-14} cm^3 s^{-1} (curves B). No significant differences are found between the results calculated at $p = 10$ Torr and 2.56 Torr, except for the times at which the maxima occur. The maxima occur slightly earlier at $p = 10$ Torr, which can be well interpreted by comparing the evolution of the VDF at both values of the pressure. The VDF for $p = 2.56$ Torr was shown in figure 3, while in figure 12 we now show this distribution calculated for 10 Torr, at the same times as before. Both VDFs have been calculated assuming reaction (12) with a rate coefficient of 10^{-12} cm^3 s^{-1}. Figure 12 shows that the VDF presents an overpopulated tail at $t = 10^{-3}$ s, whereas in figure 3 the maximum occurred in the middle of the time interval $10^{-3} < t < 10^{-2}$ s. The decrease in the time at which the maxima occur, as the pressure increases, essentially results from an enhancement of the frequencies for deactivation of the VDF by V–T exchanges associated with N_2–N_2 collisions and also from an increase in the V–V rates. As a matter of fact, the tail of the VDF is mainly controlled by V–T deactivation in collisions with $N(^4S)$ atoms [10, 17]. However, the fractional concentration $[N(^4S)]/[N_2]$ decreases by about 4.7 as the pressure increases from 2.56 Torr to 10 Torr (see figure 13), which associated with the increase of 3.9 in the gas density, produces a decrease of $\sim$1.2 in the concentration of $N(^4S)$ atoms. The V–T rates of N_2–N collisions are hence not responsible for the decrease in the time at which the maxima occur when p increases from 2.56 to 10 Torr.

Figure 13 shows the evolution of the relative concentration of $N(^4S)$ atoms in a N_2 post-discharge calculated for $p = 2.56$ Torr (curve A) and 10 Torr (curve B), with all other conditions as before, and in a microwave discharge with $\omega/(2\pi) = 2.45$ GHz, $p = 2$ Torr, $R = 0.8$ cm, $n_e = 5 \times 10^{11}$ cm^{-3} and $T_g = 1000$ K (broken curve). In this latter case, of a microwave discharge with a smaller inner radius, the sustaining reduced electric field is larger $E/N = 4.7 \times 10^{-15}$ V cm^2 ($E_e/N \sim 1.4 \times 10^{-15}$ V cm^2 for the effective reduced electric field [18]), which, associated with a higher electron density of 5×10^{11} cm^{-3}, produces a fractional concentration of $N(^4S)$ atoms of $\sim$15%. We note that such a value is one order of magnitude larger than the experimental values measured in [33] at $\omega/(2\pi) = 2.45$ GHz, which can be explained by a small frequency for wall reassociation of $N(^4S)$ atoms used in this paper, $\nu_w = \gamma\langle v\rangle/2R$ (with γ and $\langle v\rangle$ denoting the wall probability for reassociation and the average velocity of N atoms). In the conditions of the broken curve of figure 13 we have $\varnothing = 16$ mm, while in [33] the tube diameter is $\varnothing = 4.5$ mm. If further differences remain they may be justified by a lower pressure (i.e. at higher sustaining reduced electric field) and higher electron density in the conditions of this paper.

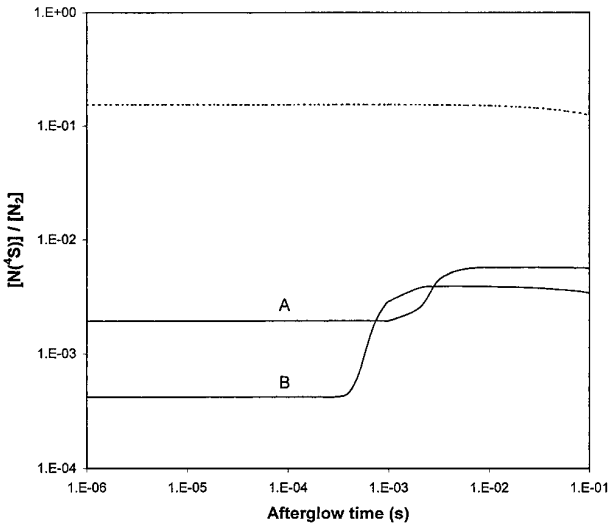

Figure 13. Temporal evolution of the fractional concentration of $N(^4S)$ atoms in the afterglow of a microwave discharge at $\omega/(2\pi) = 433$ MHz, $n_e = 10^{11}$ cm^{-3}, $R = 1.9$ cm, and $p = 2.56$ Torr (curve A) and 10 Torr (curve B). The broken curve is for $\omega/(2\pi) = 2.45$ GHz, $n_e = 5 \times 10^{11}$ cm^{-3}, $R = 0.8$ cm and $p = 2$ Torr.

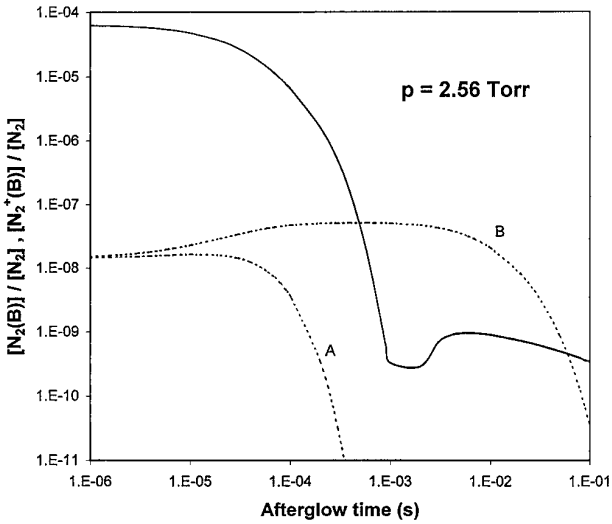

Figure 14. Temporal evolution of the fractional concentrations of $N_2(B)$ (full curve) and $N_2^+(B)$ (broken curves) in the afterglow of a microwave discharge at $\omega/(2\pi) = 433$ MHz and $p = 2.56$ Torr, when the various reactions for formation of N_2 states (discussed in section 2) are discarded from the model. The broken curves are obtained including (curve A) and neglecting (curve B) ion losses by electron–ion recombination.

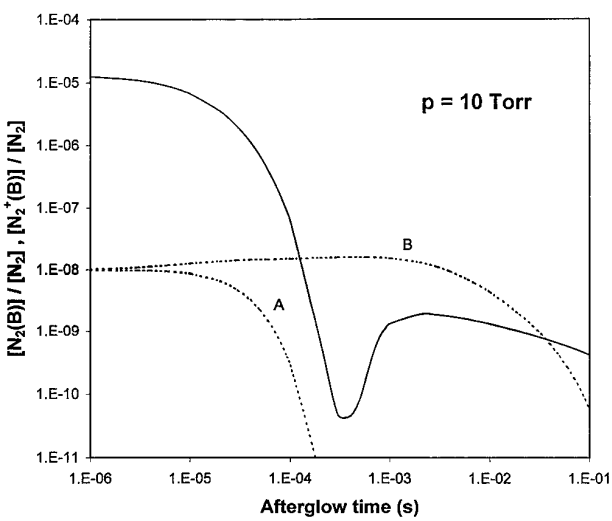

Figure 15. As in figure 14 but for $p = 10$ Torr.

The relative atomic concentration in the discharge remains with practically no modifications in the post-discharge up to $t \sim 5 \times 10^{-4}$–2×10^{-3} s. After this time, two different situations occur. For the discharge at 2.45 GHz, with a larger value of $n_e = 5 \times 10^{11}$ cm^{-3} and lower tube radius $R = 0.8$ cm, the relative concentration $[N(^4S)]/[N_2]$ remains unchanged until $t \simeq 8 \times 10^{-2}$ s, at which time it starts to decrease as a result of reassociation on the wall and to a lesser extent three-body recombination [34]. However, if we consider the situation essentially treated in this paper of a discharge at 433 MHz, with $n_e = 10^{11}$ cm^{-3} and $R = 1.9$ cm (full curves), an increase is observed in $[N(^4S)]/[N_2]$ at $t \sim 5 \times 10^{-4}$ s for $p = 10$ Torr (curve B) and at $t \sim 2 \times 10^{-3}$ s for $p = 2.56$ Torr (curve A).

To our knowledge this additional dissociation in the post-discharge has not yet been experimentally confirmed. However, it clearly arises from the model as a result of a vibrational mechanism, in which a $N_2(X,v)$ molecule in the last bound level $v = 45$ is promoted to the continuum by V–V and V–T energy exchanges where it is assumed that the molecule dissociates [35]. The different behaviours found here can be explained by the appearance of an overpopulated tail for the VDF during the relaxation process, in the post-discharge of the discharge with 433 MHz. In contrast, in the post-discharge of the discharge at 2.45 GHz, the relatively high concentration of $N(^4S)$ atoms (∼15%) produces a stronger vibrational deactivation of the VDF by V–T processes associated with N_2–N collisions. This results in a sharp depletion of the tail of the VDF and consequently dissociation by V–V and V–T processes cannot occur.

Figures 14 and 15 show the relative concentrations $[N_2(B)]/[N_2]$ and $[N_2^+(B)]/[N_2]$ in the afterglow of the microwave discharge at $p = 2.56$ Torr (figure 14) and 10 Torr (figure 15), when the reactions (5)–(8), (10), (12) for formation of N_2 electronic states in the post-discharge are discarded from the model. This means that the kinetics of the heavy species governing $N_2(B)$ and $N_2^+(B)$ states is the same as in our previous paper [10]. The increase in $N_2(B)$ concentration shown in figures 14 and 15 now results from the populating mechanism for this state by three-body recombination:

$$N(^4S) + N(^4S) + N_2 \rightarrow N_2(B\,^3\Pi_g) + N_2 \qquad (18)$$

while the enhancement of $N(^4S)$ concentration needed for the increase of $N_2(B)$ takes place via the dissociation mechanism referred to earlier involving V–V and V–T energy exchanges. The broken curves plotted in figures 14 and 15 are for $[N_2^+]/[N_2]$ in the conditions of our reference model (curves A) and neglecting electron–ion recombination in the post-discharge (curves B). In this latter case, the loss of $N_2^+(B)$ ions occurs by free diffusion only [10], which has been revealed to be an inadequate assumption. Both the rate coefficient of reaction (17), $8.27 \times 10^{-34} \times \exp(500/T_g)$ cm^6 s^{-1}, and that for

electron–ion recombination, $4.8\times10^{-7}\times(300/T_e)^{1/2}$ cm^3 s^{-1}, have been obtained from [32]. Discarding $N_2^+(B)$ losses by electron–ion recombination in the post-discharge prolongs the concentration of this species until a relatively high afterglow-time $t \sim 10^{-2}$ s (broken curves B in figures 14 and 15), preventing the appearance of the dark zone at the end of the discharge. Finally, figures 14 and 15 also show that the maximum for $[N_2^+(B)]$ in the afterglow does not occur when the reactions for producing electronic states (discussed in section 2) are discarded from the model, which clearly indicates a need for such processes.

4. Conclusions

In this paper, we have shown that the emission bands of the 1^+ and 1^- systems of N_2 observed in a flowing post-discharge, associated with the transitions $N_2(B\,^3\Pi_g \rightarrow A\,^3\Sigma_u^+)$ and $N_2^+(B\,^2\Sigma_u^+ \rightarrow X\,^2\Sigma_g^+)$, respectively, can be well interpreted by assuming the formation of N_2 electronic states in the afterglow by collisions between $N_2(X\,^1\Sigma_g^+, v)$ molecules, in highly vibrational levels, and long-lived $N(^4S)$ atoms. During the relaxation process, population inversion at the highest vth levels of $N_2(X,v)$ molecules occurs as a result of a pumping-up effect in the vibrational ladder induced by near-resonant V–V energy-exchanges. As a consequence of this, an additional amount of dissociation in the post-discharge by a purely vibrational mechanism involving V–V and V–T collisions can also occur in conditions for which the fractional concentration of dissociated atoms is small, typically for $[N(^4S)]/[N_2] < 5\times10^{-3}$, so that the VDF cannot be deactivated by V–T processes through N_2–N collisions. However, the dissociation by V–V and V–T processes has not yet been experimentally confirmed.

This study shows that only processes involving highly excited levels, as high as $v \sim 35$, can be responsible for the appearance of optical emissions in the afterglow, in a localized region downstream from the discharge after a dark zone. Here, we show that a favourable mechanism for the production of a strong and narrow maximum in the afterglow consists in the formation of the singlet state $N_2(a'\,^1\Sigma_u^-)$ by collisions between $N_2(X,v \geqslant 38)$ molecules and $N(^4S)$ atoms. On the other hand, a similar reaction for production of $N_2(A\,^3\Sigma_u^+)$ allows us to obtain only a broader peak, since this latter process involves lower vth levels. Nevertheless, we cannot conclude from this paper that the enhancement of the optical emissions in the afterglow occurs exclusively via the $N_2(a')$ state. Other mechanisms involving highly vibrational levels of $N_2(X,v)$ leading, for example, to $N_2(A)$ formation can also exist, such as in the case of reaction

$$N_2(X\,^1\Sigma_g^+, v \geqslant 39) + N(^4S) \rightarrow N_2(A\,^3\Sigma_u^+) + N(^2D). \quad (19)$$

In reaction (19), a narrow peak for $[N_2(A)]$ would also be created in the afterglow. In conclusion, various mechanisms are probable and owing to a lack of data we cannot distinguish in particular any of them. The only point that we would like to stress here is the need for highly excited levels to be involved. The uncertainty is extended to the nature of the second partner involved in the collisions, since it may be either an $N(^4S)$ atom or an $N_2(X)$ molecule. Since $[N(^4S)]/[N_2] \sim 2\times10^{-3}$ s at $p = 2.56$ Torr, the rate coefficients of the reactions with $N_2(X)$ molecules may be reduced to an upper limit of 10^{-15} cm^3 s^{-1} in order to obtain maxima of the same magnitude as those for reactions with $N(^4S)$ atoms.

Finally, the major weakness of the present paper is the assumption of a sharp cut-off in the gas temperature at the end of the discharge from $T_g = 1000$ K to 400 K. This is indeed an approximation made here with the purpose to distinguish the effects produced by the reactions that we want to study from the temperature effects. However, we note that T_g rapidly decreases in the short-lived afterglow [8, 30], so that at the point where the maxima for the emissions exist, the measured temperature is not very distant from the $T_g = 400$ K assumed here. Future work should mainly concentrate on this point in order to improve the accuracy of the model. Nevertheless, the description already seems satisfactory, on physical grounds, as it stands now.

Acknowledgment

The authors are indebted to Dr N Sadeghi for fruitful discussions during the final part of writing this paper.

References

[1] Ricard A, Oseguera-Pena J E, Falk L, Michel H and Gantois M 1990 *IEEE Trans. Plasma Sci.* **18** 940
[2] Boisse-Laporte C, Chave-Normand C and Marec J 1997 *Plasma Sources Sci. Technol.* **6** 70
[3] De Souza A R, Digiacomo M, Muzart J L R, Nahorny J and Ricard A 1999 *Europhys. Phys. J. AP* **5** 185
[4] Malvos H, Michel H and Ricard A 1994 *J. Phys. D: Appl. Phys.* **27** 1328
[5] Bockel S, Belmonte T, Michel H and Ablitzer D 1997 *Surf. Coat. Technol.* **97** 618
[6] Belmonte T, Bockel S, Michel H and Ablitzer D 1999 *Surf. Coat. Technol.* **112** 5
[7] Supiot P, Dessaux O and Goudmand P 1995 *J. Phys. D: Appl. Phys.* **28** 1826
[8] Blois D, Supiot P, Barj M, Chapput A, Foissac C, Dessaux O and Goudmand P 1998 *J. Phys. D: Appl. Phys.* **31** 2521
[9] Supiot P, Blois D, De Benedictis S, Dilecce G, Barj M, Chapput A, Dessaux O and Goudmand P 1999 *J. Phys. D: Appl. Phys.* **32** 1887
[10] Sá P A and Loureiro J 1997 *J. Phys. D: Appl. Phys.* **30** 2320
[11] Cacciatore M, Capitelli M, De Benedictis S, Dilonardo M and Gorse C 1986 *Topics in Current Physics: Nonequilibrium Vibrational Kinetics* **39** ed M Capitelli (Berlin: Springer) p 5
[12] Gordiets B, Ferreira C M, Guerra V, Loureiro J, Nahorny J, Pagnon D, Touzeau M and Vialle M 1995 *IEEE Trans. Plasma Sci.* **23** 750
[13] Brunet H, Vincent P and Rocca-Serra J 1983 *J. Appl. Phys.* **54** 4951
[14] Brunet H and Rocca-Serra J 1985 *J. Appl. Phys.* **57** 1574
[15] Berdyshev A V, Kochetov I V and Napartovich A P 1988 *Sov. J. Plasma Phys.* **14** 438
[16] Bol'shakova L G, Golubovskii Yu B, Telezhko V M and Stoyanov D G 1990 *Sov. Phys. Tech. Phys.* **35** 665
[17] Guerra V and Loureiro J 1997 *Plasma Sources Sci. Technol.* **6** 361
[18] Sá P A, Loureiro J and Ferreira C M 1992 *J. Phys. D: Appl. Phys.* **25** 960
[19] Guerra V, Sá P A and Loureiro J 2000 *Phys. Rev.* E at press
[20] Levron D and Phelps A V 1978 *J. Chem. Phys.* **69** 2260
[21] Slovetskii D I 1980 *Mechanisms of Chemical Reactions in Nonequilibrium Plasmas* (Moscow: Nauka) in Russian

[22] Heidner R F III, Sutton D G and Suchard S N 1976 *Chem. Phys. Lett.* **37** 243
[23] Gordiets B, Ferreira C M, Pinheiro M J and Ricard A 1998 *Plasma Sources Sci. Technol.* **7** 363
[24] Young R A and St John G A 1968 *J. Chem. Phys.* **48** 895
[25] Piper L G 1989 *J. Chem. Phys.* **90** 7087
[26] Cernogora G 1980 *PhD Thesis* Université Paris-Sud, Orsay-France, No 2365
[27] Fewell M P, Haydon S C and Ernest A D 1996 *Chem. Phys.* **206** 257
[28] Kim Y C and Boudart M 1991 *Langmuir* **7** 2999
[29] Yamashita T 1979 *J. Chem. Phys.* **70** 4248
[30] Foissac C, Campargue A, Kachanov A, Supiot P, Weirauch G and Sadeghi N 2000 *J. Phys. D: Appl. Phys.* **33** 2434
[31] Piper L G 1987 *J. Chem. Phys.* **87** 1625
[32] Kossyi I A, Kostinsky A Yu, Matveyev A A and Silakov V P 1992 *Plasma Sources Sci. Technol.* **1** 207
[33] Mérel P, Tabbal M, Chaker M, Moisan M and Ricard A 1998 *Plasma Sources Sci. Technol.* **7** 550
[34] Loureiro J 1991 *Chem. Phys.* **157** 157
[35] Loureiro J, Ferreira C M, Capitelli M, Gorse C and Cacciatore M 1990 *J. Phys. D: Appl. Phys.* **23** 1371